```
M. saxatilisA     LFKALGLNENDYKFGLTIVFFRPGKFAEFDHIMKSDPDHLAELVKKVNKWLIHSRWKKVQWCALSVIKLKNKILYRTSACIKMQKTVRMWLCRKKHKPRI 837
D. rerioA         LFKALGLNENDYKFGLTKVVFRPGKFAEFDQIMKSDPDHLAELVKRVNKWLICSRWKKVQWCALSVIKLKNKMLYRAQACVQMQKTVRMWLCRRKHKPRI 836
M. saxatilisB     LFKALGLNDSDFKFGLTRVFFRPGKFAEFDQIMRSDPDHLAELLRKVNTWLVCSCWKKIQWCSLSVIKLRNKMNYRALACIKIQKTVRMWLCKRKHKPRI 836
D. rerioB         LFKALGLNENDYKFGLTRVFFRPGKFAEFDQIMKSDPDHLAELVKRVNKWLVCSRWKKVQWCTLSVIKLRNKMSYRASACIRIQKTVRMWLCRRRHKPRV 839
M. musculus       LFKALGLNEVDYKFGLTQVFFRPGKFAEFDQIMKSDPDHLAELVKRVNLWLVCSRWKKVQWCSLSVIKLKNKIKYRAEACIKMQKPIRMWLCKRRHNPRI 840
R. norvegicus     LFKALGLNEVDYKFGLTKVFFRPGKFAEFDQIMKSDPDHLAELVKRVNLWLVCSRWKKVQWCSLSVIKLKNKIKYRAEACIKMQKTIRMWLCKRRHKPRI 837
S. scrofa         LFKALGLNEIDYKFGLTKVFFRPGKFAEFDQIMKSDPDHLAELVKRVNHWLICSRWKKVQWCSLSVIKLKNKIKYRAEACIKMQKTIRMWLCKRRHKPRI 837
C. familiaris     LFKALGLNEIDYKFGLTKVFFRPGKFAEFDQIMKSDPDHLAELVKRVNHWLICSRWKKVQWCSLSVIKLKNKIKYRAEACIKMQKTIRMWLCKRRHKPRI 837
H. sapiens        LFKALGLNENDYKFGLTKVFFRPGKFAEFDQIMKSDPDHLAELVKRVNHWLTCSRWKKVQWCSLSVIKLKNKIKYRAEACIKMQKTIRMWLCKRRHKPRI 837
G. gallus         LFKALGLNEIDYKFGLTKVFFRPGKFAEFDQIMKSDPDHLAELVKRVNHWLICSRWKKVQWCSLSVIKLKNKIKYRASACIKIQKTIRMWLCKRKHKPRI 837
S. purpuratus     LFHALGLDENDYQFGLTKVFFRPGKFAEFDQMMKSDPEHLRILIKKVRRWLICTRWKRGQWGTLMVIKLKNKILYRCAALVKMQSTVRMFLAMRKHRPRY 835
D. melanogsater   MFQSLNLSAKDFKFGITKVFFRPGKFVEFDRIMRSDPENMLAIVAKVKKWLIRSRWVKSALGALCVIKLRNRIIYRNKCVLIAQRIARGFLARKQHRPRY 832
                                                                                                                <- PT

M. saxatilisA     DGLVKVRNLKTRMDRFNEVVAGLKEGKQEMSKQIKDLDAAIDSLIVKIKS-TIMTRIDIDPSYHALVTRS-EHLLPALHNNN--KEEEERERLRRIEEEM 933
D. rerioA         DGLVKAQNLKKRMEKLNEVVSGLKEGKQEMSKHMQDLDSSIDAHIRKIKS-IVMSRMDIDHEHQALVTRS-QELLSAMQKKK--QEEEEMERLKRIQEEM 932
M. saxatilisB     DGMVKVRNLKKHMERFNKVVNGLKEGKQEMAKQVQELAASIDALLTKIKA-TVMTRKDIDTEYQGLVKRS-EQLLSSMQKKK--QEEEETERLKHIEEEM 932
D. rerioB         DGLVKVKNLRKRMERFNEAVNGLKEGKAEMSKQIEELAASTDALMAKIKT-TVMSRKEIEQEYEGLVKRS-EQLLSSMQKKK--QEQEETERLKHIQEZM 935
M. musculus       DGLVKVGTLKKRLDKFNEVVSALKDGKPEVNRQIKNLEISIDALMAKFTS-TMMTREQIQKEYDALVKSS-EDLLSALQKKK--QQEEEAERLRRIQEEM 936
R. norvegicus     DGLVKVGTLKKRLDKFNEVVSALKDGKPEVNRQIKDLEISIDALMAKIKS-TMMTREQIQKEYDALVKSS-EDLLSALQKKK--QQEEEAERLRRIQEEM 933
S. scrofa         DGLVKVGTLKKRLDKFNEVVSALKDGKQEMSKQVKDLEISIDALMAKIKS-TMMTREQIQKEYDALVKSS-AVLLSALQKKK--QQEEEAERLRRIQEEM 933
C. familiaris     DGLVKVGTLKKRLDKFNEVVSALKDGKLEMNKQVKDLEISIDALMAKIKS-TMMTREQIRREYDALVKSS-EELLSALQKKK--QQEEEAERLKRIQEEM 933
H. sapiens        DGLVKVGTLKKRLDKFNEVVSVLKDGKPEMNKQIKNLEISIDTLMAKIKS-TMMTQEQIQKEYDALVKSS-EELLSALQKKK--QQEEEAERLRRIQEEM 933
G. gallus         DGLIKVRTLKKRLDKFNEVVSALKEGKAETSKQIKELEYSIDASMTKIKT-TMMTREQIMKEYDALVRSS-EQLLSALQKKK--QQEEEAERLRRIQEEM 933
S. purpuratus     RSLKQVNTLSKELDKLAQVAKTVKD--KVAQQQVAATSKALQDLIIKIKT-TIMTRRQMEDAYLNLSNQMRKQLLDLINKKK--AEDAEADRLRKIQEEM 930
D. melanogsater   QGIGKINKIRTNTLKTIEIASGLKMGREEIISGVNDIYRQIDDAIKKIKMNPRITQREMDSMYTVVMANMNKLTVDLNTKLKEQQQAEEQERLRKIQEAL 932
                                                                                  PT-><-MT

M. saxatilisA     EREKKRREEEEQRRKQE-----------EEDRRLKAEMEVKRKQEEEERKRREEEERRIQVEMELQLQAEREEDAARQTILEQERRDRELALRIAQSEAE 1022
D. rerioA         EKERKRREEEEQKRKRE-----------EEERRQKAEMELKRKQEEEERKKREEEERKLQEEMELQLEAEREQETSRQAVLEQERRDRELALRIAQSEAE 1021
M. saxatilisB     EKERKRREKEEQRRKQE-----------EEDRRLKAEMELKRKQEEEDRKKREEEEKVIQAELEIQLALEREEQAQRTTILEQEKRDRELAMRIAQSEAE 1021
D. rerioB         EKERKRHEEEEQLRKQE-----------EEDRRMKSEMEQKRKQEEEERKKREEEERVLQAELEMQLALDREEETQRQTILEQERRDRELAMRIAQNEAE 1024
M. musculus       EKERKRREEDEERRRKE-----------EEERRMKLEMEPKRKQEEEERKKREDDEKRIQSEVEAQLARQREEESQQQAVLAQECRDRELALRIAQNESE 1025
R. norvegicus     EKERKRREEDEQRRRKE-----------EEERRMKLEMEVKRKQEEEERKKREDDEKRIQAEVEAQLARQREEESQQQAVLAQECRDRELALRIAQNESE 1022
S. scrofa         EKERKRREEDEQRRRKE-----------EEERRMKLEMEAKRKQEEEERKKREDDEKRIQAEVEAQLARQREEESQQQAVLEQERRDRELALRIAQSEAE 1022
C. familiaris     EKERKRREEDERRRRKE-----------EEERRMKLEMEAKRKQEEEERKKREDDEKRIQAEVEEQLARQREEESQQQAVLEQERRDRELALRIAQSEAE 1022
H. sapiens        EKERKRREEDEKRRRKE-----------EEERRMKLEMEAKRKQEEEERKKREDDEKRIQAEVEAQLARQKEEESQQQAVLEQERRDRELALRIAQSEAE 1022
G. gallus         EKERKRREEEEKRRRKE-----------EEERRLKSEIEAKRKQEEEERKKREEEEKRIQAEIEAQLAREREEETQHQAILEQERRDRELAMRIAQTGAE 1022
S. purpuratus     ERERKRREEEERKRKAEQEERERKKLQEEEERKLKAEMEAKRLREEEELRIQLEEEQKKLAAERKQIEADRQKLEEMQRQAEEEQRRREEQERRDYELAQ 1030
D. melanogsater   EAERAAKEAEEQRQREE-----------IENKRLKAEMETRRKAAEAQRLRQEEEDRRAALALQEQLEKEAKDDAKYRQQLEQERRDHELALRLANESNG 1021
                                                                  MT-><-DT
```

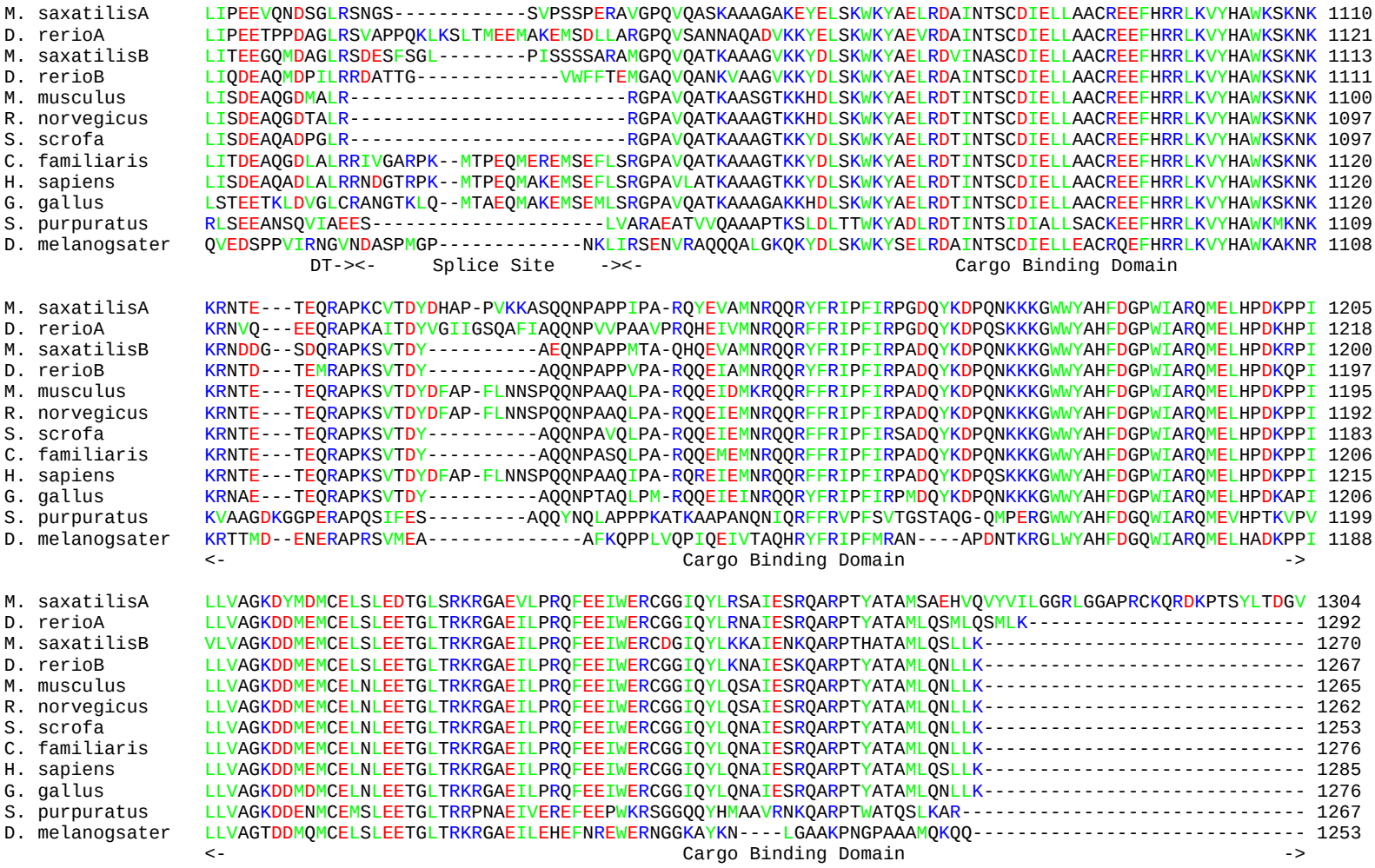
M. saxatilisA LIPEEVQNDSGLRSNGS----------SVPSSPERAVGPQVQASKAAAGAKEYELSKWKYAELRDAINTSCDIELLAACREEFHRRLKVYHAWKSKNK 1110
D. rerioA LIPEETPPDAGLRSVAPPQKLKSLTMEEMAKEMSDLLARGPQVSANNAQADVKKYELSKWKYAEVRDAINTSCDIELLAACREEFHRRLKVYHAWKSKNK 1121
M. saxatilisB LITEEGQMDAGLRSDESFSGL--------PISSSSARAMGPQVQATKAAAGVKKYDLSKWKYAELRDVINASCDIELLAACREEFHRRLKVYHAWKSKNK 1113
D. rerioB LIQDEAQMDPILRRDATTG----------VWFFTEMGAQVQANKVAAGVKKYDLSKWKYAELRDAINTSCDIELLAACREEFHRRLKVYHAWKSKNK 1111
M. musculus LISDEAQGDMALR------------------------RGPAVQATKAASGTKKHDLSKWKYAELRDTINTSCDIELLAACREEFHRRLKVYHAWKSKNK 1100
R. norvegicus LISDEAQGDTALR------------------------RGPAVQATKAAAGTKKHDLSKWKYAELRDTINTSCDIELLAACREEFHRRLKVYHAWKSKNK 1097
S. scrofa LISDEAQADPGLR------------------------RGPAVQATKAAAGTKKYDLSKWKYAELRDTINTSCDIELLAACREEFHRRLKVYHAWKSKNK 1097
C. familiaris LITDEAQGDLALRRIVGARPK--MTPEQMEREMSEFLSRGPAVQATKAAAGTKKYDLSKWKYAELRDTINTSCDIELLAACREEFHRRLKVYHAWKSKNK 1120
H. sapiens LISDEAQADLALRRNDGTRPK--MTPEQMAKEMSEFLSRGPAVLATKAAAGTKKYDLSKWKYAELRDTINTSCDIELLAACREEFHRRLKVYHAWKSKNK 1120
G. gallus LSTEETKLDVGLCRANGTKLQ--MTAEQMAKEMSEMLSRGPAVQATKAAAGAKKHDLSKWKYAELRDTINTSCDIELLAACREEFHRRLKVYHAWKSKNK 1120
S. purpuratus RLSEEANSQVIAEES----------------------LVARAEATVVQAAAPTKSLDLTTWKYADLRDTINTSIDIALLSACKEEFHRRLKVYHAWKMKNK 1109
D. melanogsater QVEDSPPVIRNGVNDASPMGP----------NKLIRSENVRAQQQALGKQKYDLSKWKYSELRDAINTSCDIELLEACRQEFHRRLKVYHAWKAKNR 1108
DT-><- Splice Site -><- Cargo Binding Domain
M. saxatilisA KRNTE---TEQRAPKCVTDYDHAP-PVKKASQQNPAPPIPA-RQYEVAMNRQQRYFRIPFIRPGDQYKDPQNKKKGWWYAHFDGPWIARQMELHPDKPPI 1205
D. rerioA KRNVQ---EEQRAPKAITDYVGIIGSQAFIAQQNPVVPAAVPRQHEIVMNRQQRFFRIPFIRPGDQYKDPQSKKKGWWYAHFDGPWIARQMELHPDKHPI 1218
M. saxatilisB KRNDDG--SDQRAPKSVTDY----------AEQNPAPPMTA-QHQEVAMNRQQRYFRIPFIRPADQYKDPQNKKKGWWYAHFDGPWIARQMELHPDKRPI 1200
D. rerioB KRNTD---TEMRAPKSVTDY----------AQQNPAPPVPA-RQQEIAMNRQQRYFRIPFIRPADQYKDPQNKKKGWWYAHFDGPWIARQMELHPDKQPI 1197
M. musculus KRNTE---TEQRAPKSVTDYDFAP-FLNNSPQQNPAAQLPA-RQQEIDMKRQQRFFRIPFIRPADQYKDPQNKKKGWWYAHFDGPWIARQMELHPDKPPI 1195
R. norvegicus KRNTE---TEQRAPKSVTDYDFAP-FLNNSPQQNPAAQLPA-RQQEIEMNRQQRFFRIPFIRPADQYKDPQNKKKGWWYAHFDGPWIARQMELHPDKPPI 1192
S. scrofa KRNTE---TEQRAPKSVTDY----------AQQNPAVQLPA-RQQEIEMNRQQRFFRIPFIRSADQYKDPQNKKKGWWYAHFDGPWIARQMELHPDKPPI 1183
C. familiaris KRNTE---TEQRAPKSVTDY----------AQQNPASQLPA-RQQEMEMNRQQRFFRIPFIRPADQYKDPQNKKKGWWYAHFDGPWIARQMELHPDKPPI 1206
H. sapiens KRNTE---TEQRAPKSVTDYDFAP-FLNNSPQQNPAAQIPA-RQREIEMNRQQRFFRIPFIRPADQYKDPQSKKKGWWYAHFDGPWIARQMELHPDKPPI 1215
G. gallus KRNAE---TEQRAPKSVTDY----------AQQNPTAQLPM-RQQEIEINRQQRYFRIPFIRPMDQYKDPQNKKKGWWYAHFDGPWIARQMELHPDKAPI 1206
S. purpuratus KVAAGDKGGPERAPQSIFES---------AQQYNQLAPPPKATKAAPANQNIQRFFRVPFSVTGSTAQG-QMPERGWWYAHFDGQWIARQMEVHPTKVPV 1199
D. melanogsater KRTTMD--ENERAPRSVMEA----------AFKQPPLVQPIQEIVTAQHRYFRIPFMRAN----APDNTKRGLWYAHFDGQWIARQMELHADKPPI 1188
<- Cargo Binding Domain ->
M. saxatilisA LLVAGKDYMDMCELSLEDTGLSRKRGAEVLPRQFEEIWERCGGIQYLRSAIESRQARPTYATAMSAEHVQVYVILGGRLGGAPRCKQRDKPTSYLTDGV 1304
D. rerioA LLVAGKDDMEMCELSLEETGLTRKRGAEILPRQFEEIWERCGGIQYLRNAIESRQARPTYATAMLQSMLQSMLK---------- 1292
M. saxatilisB VLVAGKDDMEMCELSLEETGLTRKRGAEILPRQFEEIWERCDGIQYLKKAIENKQARPTHATAMLQSLLK---------- 1270
D. rerioB LLVAGKDDMEMCELSLEETGLTRKRGAEILPRQFEEIWERCGGIQYLKNAIESKQARPTYATAMLQNLLK---------- 1267
M. musculus LLVAGKDDMEMCELNLEETGLTRKRGAEILPRQFEEIWERCGGIQYLQSAIESRQARPTYATAMLQNLLK---------- 1265
R. norvegicus LLVAGKDDMEMCELNLEETGLTRKRGAEILPRQFEEIWERCGGIQYLQSAIESRQARPTYATAMLQNLLK---------- 1262
S. scrofa LLVAGKDDMEMCELNLEETGLTRKRGAEILPRQFEEIWERCGGIQYLQNAIESRQARPTYATAMLQNLLK---------- 1253
C. familiaris LLVAGKDDMEMCELNLEETGLTRKRGAEILPRQFEEIWERCGGIQYLQNAIESRQARPTYATAMLQNLLK---------- 1276
H. sapiens LLVAGKDDMEMCELNLEETGLTRKRGAEILPRQFEEIWERCGGIQYLQNAIESRQARPTYATAMLQSLLK---------- 1285
G. gallus LLVAGKDDMDMCELNLEETGLTRKRGAEILPRQFEEIWERCGGIQYLQNAIESRQARPTYATAMLQNLLK---------- 1276
S. purpuratus LLVAGKDDENMCEMSLEETGLTRRPNAEIVEREFEEPWKRSGGQQYHMAAVRNKQARPTWATQSLKAR---------- 1267
D. melanogsater LLVAGTDDMQMCELSLEETGLTRKRGAEILEHEFNREWERNGGKAYKN----LGAAKPNGPAAAMQKQQ---------- 1253
<- Cargo Binding Domain ->

Supplemental Figure 1: Sequence Alignment of Myosin VI Tail Domains. ClustalW was used to create a sequence alignment of myosin VI tail domains from various organisms. The residues were color coded as in Fig.1 and the domain boundaries labelled beneath the sequence.

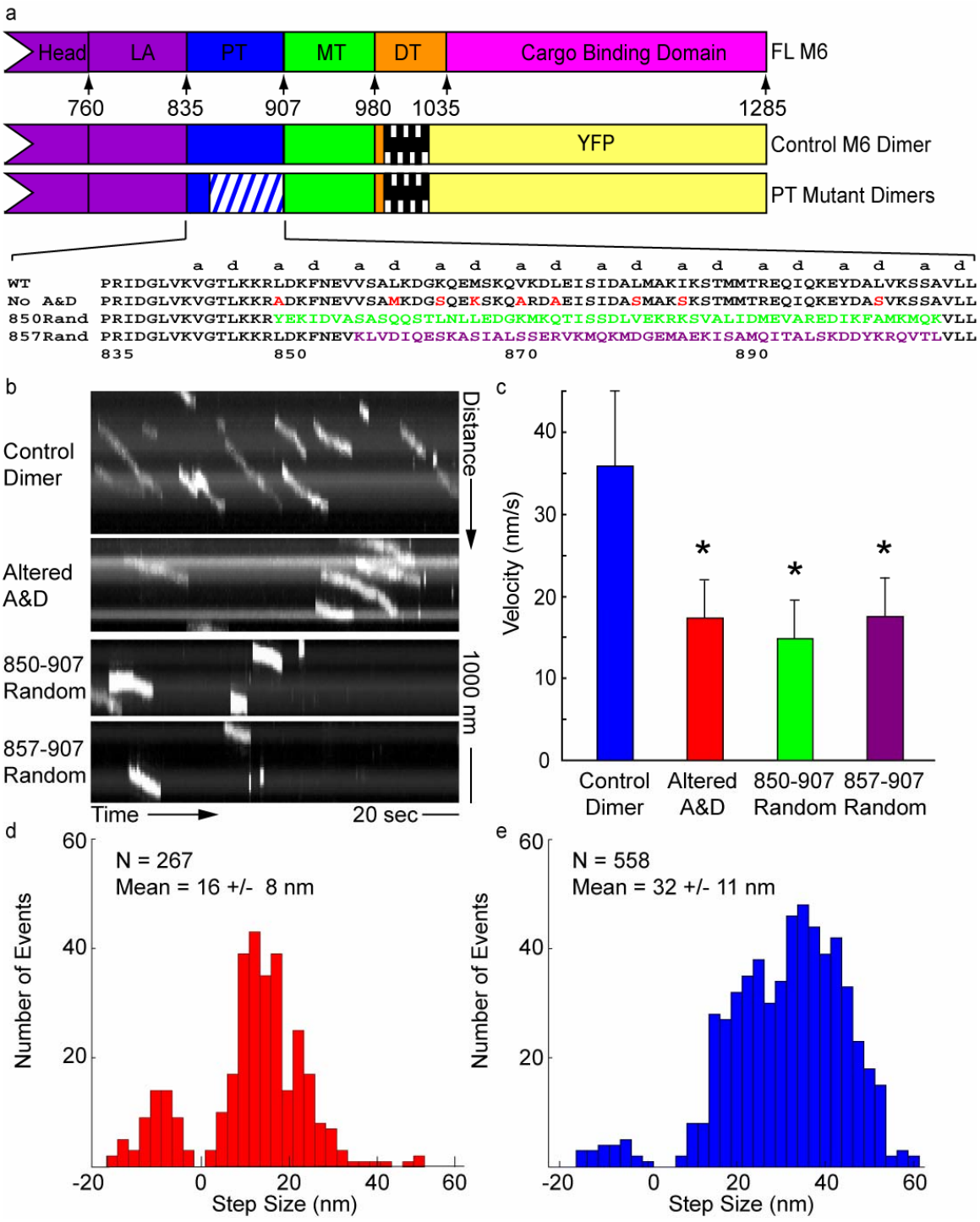

Supplemental Figure 2: Proximal tail mutant motility assays. a, The domain structure of M6 with labelled domain boundaries juxtaposed to the control M6 dimer and the PT mutants. The sequence of the PT in the three M6 PT mutants is displayed next to the native sequence, with the putative coiled coil heptad pattern labelled at the *a* and *d*

positions shown. The Altered A&D construct has nine point mutations at the proposed *a* and *d* core positions of the heptad repeat, which removed all predicted propensity to form a coiled coil. The other two M6 constructs have the majority of the PT replaced with randomized sequences. One replaced residues 850-907 with a new sequence comprised of the same amino acids but in a random order (850-907 Random). Another replaced residues 857-907 in the same manner with a different random order (857-907 Random). This randomization was intended to preserve any worm like chain properties of the sequence by holding the number of prolines and glycines constant and maintaining the same number of charged residues. b, Sample kymographs for control M6 dimer and the mutant dimeric constructs showing the position of a fluorescent processive motor along the length of an actin filament over time in 80 μM ATP. c, Observed velocities of the four motors, Control M6 dimer (blue) = 36 +/- 9 nm s^{-1} (n=107), Altered A&D (red) = 17 nm s^{-1} +/- 4 (n=105), 850-907 Random (green) = 15 +/- 5 nm s^{-1} (n=115), 857-907 Random (purple) = 18 +/- 5 nm s^{-1} (n=87). The expected velocity based on previously measured ATPase rates and step sizes for the control M6 dimer is 40 nm s^{-1}, in good agreement with the control M6 dimer measurements reported here, but higher than the mutant dimer constructs. Asterisks indicate significant differences from control in a Dunnett's test (See methods). d and e, Histograms of measured processive step sizes for 850-907 Random (d) and control M6 dimer (e) in a dual beam optical trap assay. The mean forward step size ((-) end directed) is listed on the figure, and the mean backwards step size ((+) end directed) was 11 +/- 5 nm (n=60) for 850-907 Random and 8.5 +/- 4.3 nm (n=21) for the control M6 dimer. Computing the mean rate of stepping and multiplying by the mean step size of 850-907 Random provides an estimate of the expected velocity of the motor, which corresponds well to the measured velocities in the TIRF motility assays (16 nm s^{-1} vs. 18 nm s^{-1}).

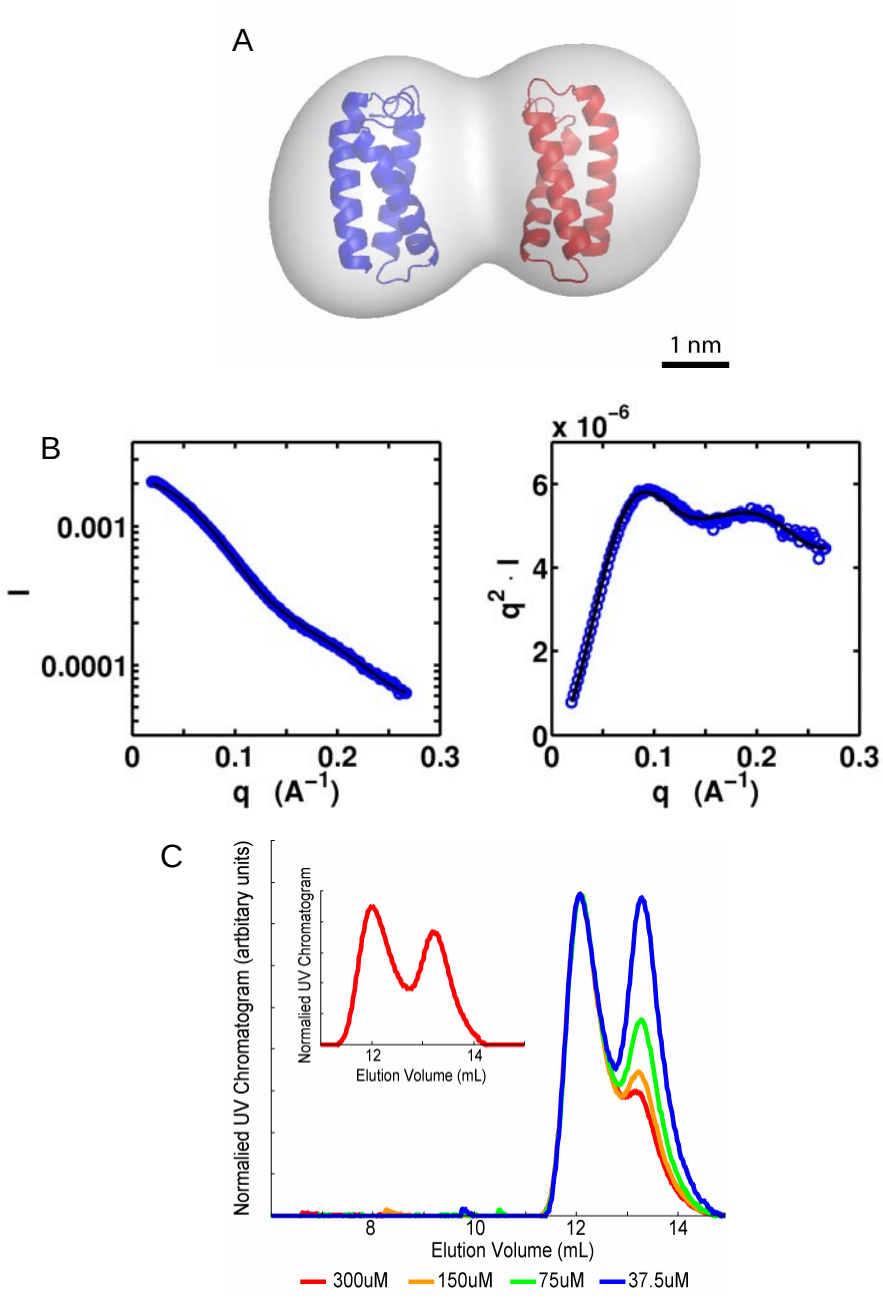

Supplemental Figure 3: Proximal tail size and dimerization state. a, GASBOR reconstruction for dimeric PT showing a compact structure indicating that this dimer cannot be a coiled coil. Two copies of the rosetta structure prediction of the PT have been manually aligned into the SAXS envelope showing that the predicted structure is compatible with the data. This rosetta prediction fits with many other aspects of the data and most likely represents a good estimate of the PT structure. The three helix bundle

would be stiff enough to act as a lever arm while maintaining the N and C-termini at opposite ends, a requirement for a lever arm extension. The predicted radius of gyration for the molecule is 1.3 nm in very good agreement with the measured hydrodynamic radius of 1.6 nm, with the difference being accounted for by a one water molecule thick hydration layer. The number of α-helical peptide bonds in the backbone is in good agreement with the number calculated from the CD data. The end to end distance of the three helix bundle is 3 nm, which is the amount that the PT extends the calmodulin based lever arm. b, Experimental SAXS profile at a protein concentration of ~200 μM (blue circles) and fits to the data using the structure reconstruction algorithm GASBOR with dimeric (P2) symmetry (black solid line). Scattering intensities are shown as log(I) as a function of q (left) and in Kratky representation [$q^2 \times I$ as a function of q] (right). The number of points in the experimental profiles was reduced for clarity. c, Chromatograms from gel filtration runs of various concentrations of PT dimer were normalized to the first peak. As the loaded concentration was reduced, the relative abundance of the second peak increased, leading to the conclusion that the first peak is a dimer peak and the second peak is a monomer. The inset shows the dimer peak from the 300 μM load that was re-run on the same column immediately after being separated from the monomer peak. If the peaks resulted from two different species, then this dimer peak should elute as a single species. However, if a dimerization process is occurring then it should re-equilibrate and produce both peaks. Two peaks are seen indicating that re-equilibration occurred. The hydrodynamic radius reported in Table 1 is from analysis of the second peak. The 150 μM load produces approximately equal molar amounts of monomer and dimer, which allows for the estimate of ~150 μM for the K_d. SAXS profiles for the PT construct show a systematic concentration dependence below a protein concentration of ~ 200 μM, consistent with a monomer-dimer equilibrium (data not shown). Guinier analysis of the SAXS data at ~ 200 μM PT gave a radius of gyration of 2.2 ± 0.2 Å and a molecular weight estimate of 17 ± 2 kDa, consistent with a dimer.

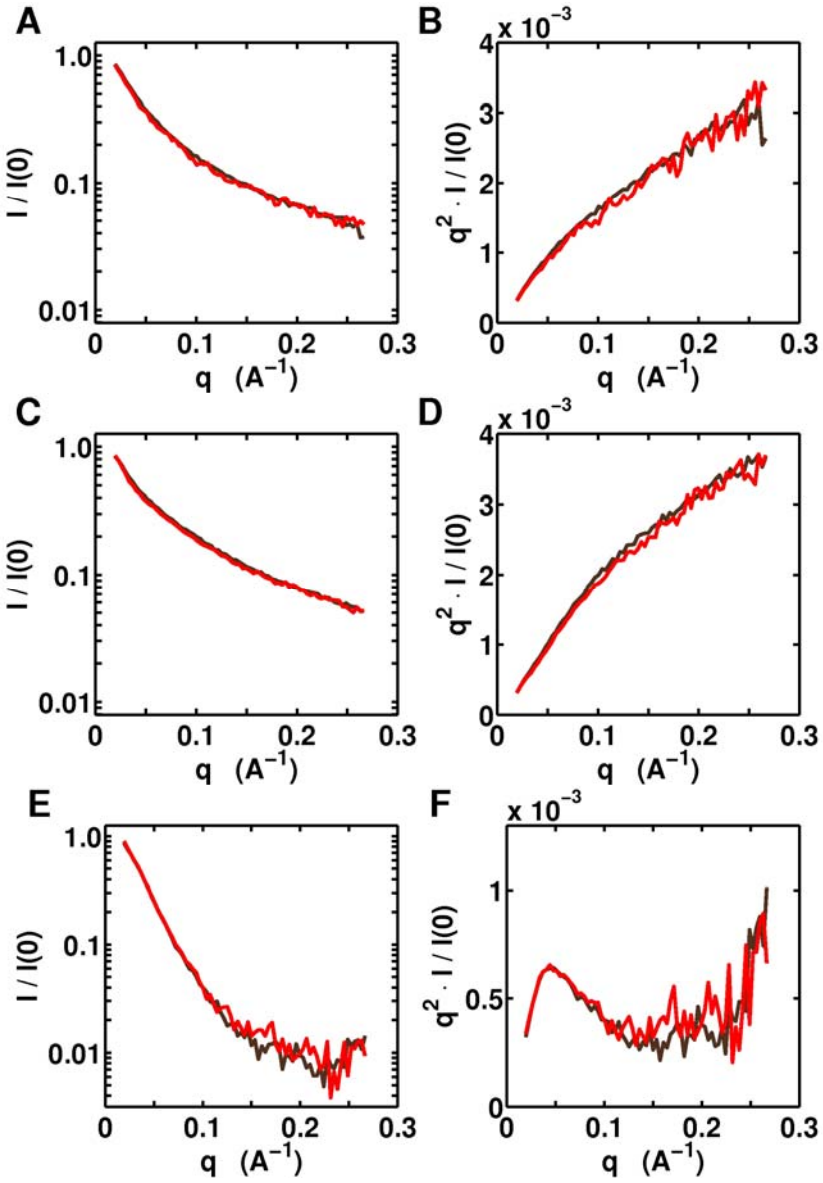

Supplemental Figure 4. SAXS profiles for the MT-DT (A and B), PT-DT (C and D), and full length M6 (E and F) constructs at low (red) and high (brown) protein concentrations. The protein concentrations are 3 (red) and 6 (brown) mg/ml for the MT-DT and PT-DT constructs (A-D), and 0.45 (red) and 0.9 (brown) mg/ml for full length M6. Scattering intensities are normalized by forward scattering intensity, I(0), and are shown as log(I) as a function of q (left) and in Kratky representation [$q^2 \times I$ as a function of q] (right).

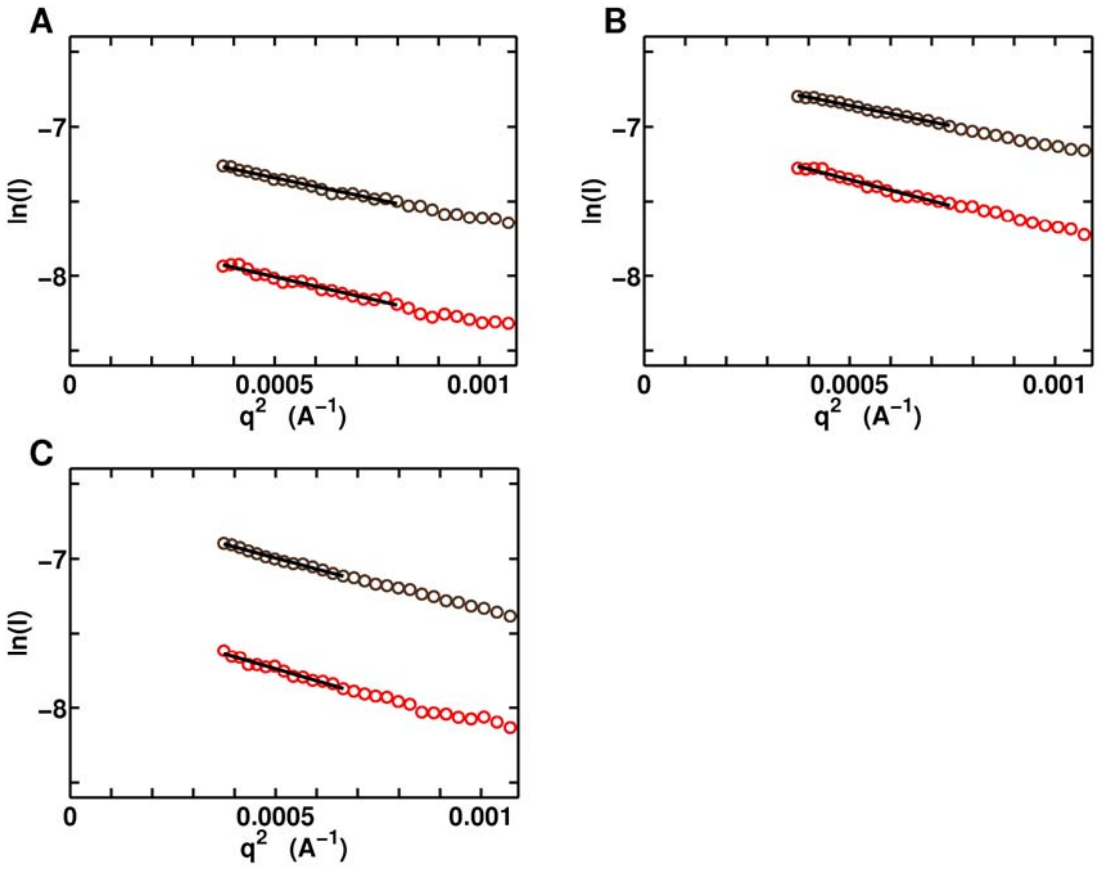

Supplemental Figure 5. Guinier analysis of SAXS profiles for the MT-DT (A), PT-DT (B), and full length M6 (C) constructs at low (red) and high (brown) protein concentrations (same protein concentrations as in Supplementary Figure 3). Data are shown in Guinier representation [ln(I) as a function of q] (circles) and Guinier fits are indicated by the solid lines. The radii of gyration are determined from the slope of the Guinier fit to be 4.3 ± 0.2, 4.4 ± 0.2, and 4.6 ± 0.3 nm, respectively.

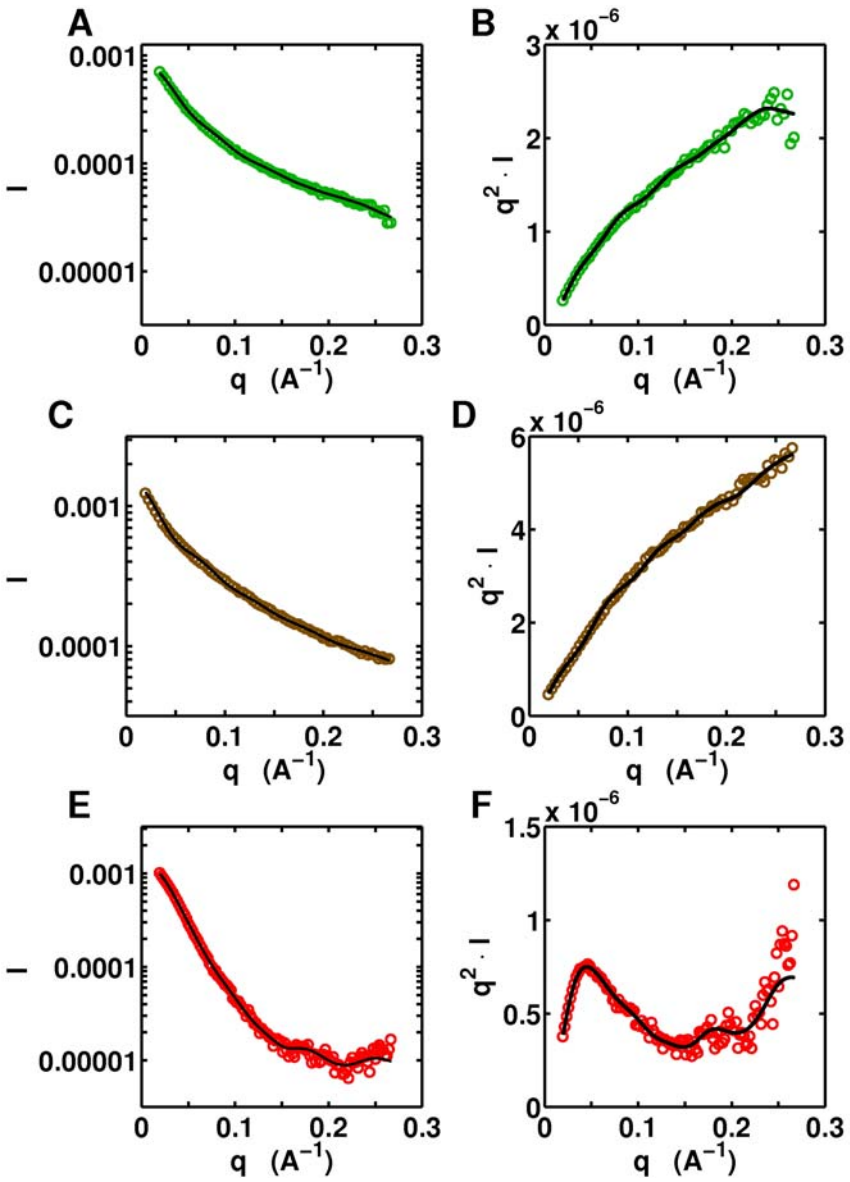

Supplemental Figure 6. *Ab initio* structure reconstruction fits to the experimental SAXS profiles. Experimental scattering profiles for the MT-DT (A and B, green circles), PT-DT (C and D, brown circles), and full length M6 (E and F, red circles) constructs and fits to the data (black solid lines) using the structure reconstruction algorithms GASBOR (A-D) and DAMMIN (E and F). Scattering intensities are shown as log(I) as a function of q (left) and in Kratky representation [$q^2 \times I$ as a function of q] (right) as in Supplementary Figure 4. The number of points in the experimental profiles was reduced for clarity.

Supplementary Methods

Expression of Tail Domain Constructs: The appropriate sequences from the human myosin VI (M6) cDNA from the HUGE database[1] (GenBank Accession No. AB002387) were PCR amplified, with the primers introducing a BamHI site at the 5' end and a stop codon and EcoRI site at the 3' end, and cloned into a modified pET28a vector (EMD Chemicals, San Diego CA). The modified vector contained a His_6 tag, maltose binding protein and a TEV protease cleavage site 5' to the cloning site. We designed the constructs such that after TEV cleavage the M6 domain would contain only a GlyGlySer N-terminal addition. Proteins were expressed in *E.coli* Rosetta (DE3) cells (EMD Chemicals, San Diego CA) by growing to an OD_{600} of 0.8-1.2 in terrific broth media. After 4 hours of protein induction with 0.5 mM IPTG at 20ºC, cells were harvested by spinning at 4000 × *g* for 20 minutes. Cells were resuspended in lysis buffer (20 mM phosphate pH 7.4, 0.5 M NaCl, 10 mM imidazole pH 7.5, 10% (v/v) glycerol plus complete protease inhibitor tabs (Roche) and lysed by adding lysozyme (Sigma) to 1 mg ml^{-1}, incubating for 15 minutes, and sonicating. Lysates were clarified by centrifugation at 100,000 × *g* for 30 minutes and supernatants were bound to Ni-NTA resin (Qiagen) for 30 minutes. The resin was washed with 8 column volumes of 20 mM phosphate pH 7.4, 0.5 M NaCl, 20 mM imidazole pH 7.5 buffer and eluted with 20 mM phosphate pH 7.4, 0.5 M NaCl, 0.5 M imidazole pH 7.5 buffer. Elutions were dialysed into 10 mM Tris pH 8.5 in the presence of TEV protease (1 to 100 by weight) overnight to cleave the His_6 and MBP portions from the M6 domains. M6 domains were further purified by running the cleavage reaction over a Ni-NTA column to remove His_6 containing fragments, running a MonoQ column (GE Healthcare, Piscataway NJ) with 10 mM Tris pH 8.5 buffer, and 10 mM Tris pH 8.5 plus 1 M NaCl buffer forming the gradient, and running a superdex 200 column in either CD buffer (10 mM phosphate pH 7.4, 25 mM NaCl) or scattering buffer (10 mM phosphate pH 7.4, 150 mM NaCl). For the PT CD experiments only the second

peak from the gel filtration was used to ensure the protein was monomeric. For the oxidized dimer of the MT-DT a GlyGlyCys sequence was added to the C-terminus and the constructs were dialyzed against the CD buffer overnight to create disulfide bridges prior to running the final gel filtration column which separated monomeric and dimeric species.

Expression of Motor Domain Containing Constructs: The porcine control M6 dimer construct described previously[2] was modified to create the mutants, and the full length M6 was made using the cDNA listed above. M6 Altered A&D, 850-907 Random, and 857-907 Random sequences were synthesized by DNA 2.0 (Menlo Park CA) and cloned in the control dimer background. The protein sequences are described in the supplementary Figure 2. M6 MT Locked was made by overlapping PCR[3] with a GCN4 sequence was inserted in place of residues 919 to 950 of the control dimer. A C-terminal GlyGlyAspTyrLysAspAspAspAspLys FLAG tag was added, except in full length M6 where it was placed at the N-terminus, and these sequences were placed under the control of the polyhedron promoter of the pFastBac Dual vector (Invitrogen). The vector also contained sea urchin calmodulin (P05934) under the control of the p10 promoter. Recombinant baculo-viruses were created per the Invitrogen protocol. Sf9 cells were infected with virus and cells harvested 66-78 hours post infection. Proteins were purified as described in De La Cruz *et al*.[2] Briefly this entailed lysing cells using 200 mM NaCl, 4 mM $MgCl_2$, 20 mM Imidazole, pH 7.5, 0.5 mM EDTA, 1 mM EGTA, 0.5% (v/v) Igepal, 7% (w/v) Sucrose, 5 mM DTT, 2 mM ATP plus complete protease inhibitor tabs (Roche), clarifying by centrifugation for 1 hour at 200,000 × *g*, binding to FLAG M2 affinity gel (Sigma), washing with 20 column volumes of 150 mM KCl, 20 mM imidazole, pH 7.5, 5 mM $MgCl_2$, 3 mM DTT, 1 mM EDTA, 1 mM EGTA, 3 mM ATP, and eluting with wash buffer plus 0.4 mg mL^{-1} FLAG peptide. For scattering analysis, full length M6 was gel filtered using a superdex 200 column in scattering buffer. For all

constructs absorbance at 280 nm in 6 M guanidinium chloride was used to determine the protein concentration.

Circular dichroism measurements: CD Spectra were acquired using an Aviv 62DS instrument (Aviv Biomedical, Lakewood NJ) with a 1 mm path length quartz cell in CD buffer. Spectra were taken at 10ºC with data collected every 1 nm with a 20 second averaging time, and are the average of 3 repeat scans. Concentrations ranged from 1 to 17 μM. Melt data was collected every 1ºC with a 30 s averaging time and a 2 minute equilibration. In all cases the reverse melt showed at least 90% reversibility. Raw data was converted to mean residue ellipticity using the following relationship:

$$[\theta] = \frac{\theta}{10 \times c \times n \times l}$$

Where θ is raw signal in mDeg, l is pathlength in cm, n is number of residues and c is concentration in moles per liter. The percent helical content was determined using the methods described in Chen *et al*.[4].

Multiple angle light scattering measurements: In solution molecular weights were determined using a size exclusion chromatography system coupled to a multiple angle light scattering detector. 100 μl of protein samples at >3 mg ml^{-1} were injected onto a Shodex Protein KW-803 HPLC column at a flow rate of 0.5 ml min^{-1}. The columns were equilibrated in scattering buffer. Protein concentrations were determined with an Optilab rEX refractive index detector and scattering was detected with a Dawn 18 angle MALS light scattering instrument (Wyatt Technology Corporation). Molecular weights were determined y the ASTRA software that accompanies the instrument. In all cases only detectors 7-15 of the 18 total (detector angles 57º, 64º, 72º, 81º, 90º, 99º, 108º, 117º, and

126º) were used for the final determination of the molecular mass. Other detectors were excluded due to low signal intensity.

MALDI-TOF mass spectrometry analysis: Protein samples at ~10 μM in CD buffer were mixed in a 2:1 ratio with sinapinic acid and spotted onto a stainless steel MALDI plate. Analysis was conducted on a Voyager-DE RP (Applied Biosystems, CA) instrument in positive linear mode with the following parameters: Accelerating Voltage 25 kV, Grid Voltage 90.5%, Guide Wire 0.1%, Delay Time 600, Laser Intensity 3000-3200.

Dynamic light scattering measurements: Measurements were made using a DynaPro instrument (Protein Solutions, Charlottesville VA) running Dynamics version 6 software. Samples at 1 – 10 mg ml^{-1} in scattering buffer were assayed at 25ºC with an acquisition interval of 10 sec. Samples were spun at ~15,000 × *g* for 10 minutes immediately prior to analysis. Results were derived form the analysis performed by the Dynamics software that accompanies the instrument using a regularization fit and with PBS selected as the buffer.

Analytical gel filtration: Proteins were concentrated to 10 – 300 μM and loaded onto a 25 ml superdex 200 (GE Healthcare, Piscataway NJ), equilibrated in scattering buffer, in a total volume of 100 μl. The elution volume was determined from the average of at least three runs and converted to hydrodynamic radius using a standard curve developed with blue dextran 2000, BSA, ovalbumin, chymotrypsinogen, ribonucleaseA, and vitamin B12 also in scattering buffer.

SAXS measurements: Measurements were carried out at the XOR/BESSRC undulator beam line 12-ID of the Advanced Photon Source, Argonne, IL, employing a sample-detector distance of 2 m and CCD detector read out (MAR USA). The data were

collected using a custom-made sample cell[5] at an X-ray energy of 12 keV. Details of the beam line are as described previously[6,7,5].

Protein samples were dissolved in 20 mM Na-phosphate buffer, pH 7.4, with 25 mM NaCl added and centrifuged at 10,000 × *g* for 10 min prior to measurement. For each data point, three exposures of 0.5 s each were obtained, data were image corrected, normalized by incident flux and circularly averaged. The three profiles for each condition were averaged to improve signal quality. Appropriate buffer profiles were collected using identical procedures and subtracted for background correction. The data showed no signs of radiation damage, as tested by comparing scattering profiles of subsequent exposures on the same sample (data not shown).

SAXS data analysis: Scattering intensities as a function of the momentum transfer q ($q = 4 \pi \sin(\theta)/\lambda$, where 2θ is the total scattering angle and λ is the X-ray wavelength) were obtained at different protein concentrations. The SAXS profiles for the MT-DT, PT-DT, and full length M6 constructs are superimposable after scaling by forward scattering intensity, suggesting that there are no detectable aggregation or interparticle interference effects (Supplemental Fig. 4). Radii of gyration were determined from Guinier analysis of the low q scattering data[8] (Supplemental Fig. 5). The radii of gyration obtained from Guinier analysis agree within experimental errors with the values from the real space distribution function P(r) computed using the regularized transform method implemented in the program GNOM[9].

SAXS structure reconstructions: The programs DAMMIN[10] and GASBOR[11] were used to construct 3-D bead models that fit the scattering data. Both programs employ a simulated annealing procedure and a compactness criterion. Ten independent DAMMIN and GASBOR runs were performed for each scattering profile, using default parameters,

the "slow" mode for DAMMIN, no symmetry assumptions (P1 symmetry), and the full recorded scattering profiles. The models resulting from independent runs were superimposed and compared using the program SUPCOMB[12] based on the Normalized Spatial Discrepancy (NSD) criterion. Models with NSD values < 1 are considered similar. For all data presented in the main text, the ten independent repeat runs yielded models with pairwise NSD values < 1, indicating that the algorithms converged reproducibly to similar structures. The ten independent structures for each scattering profile were subsequently averaged and "filtered" consensus models were computed using the program DAMAVER with default settings[13]. Consensus models constructed with DAMMIN and GASBOR gave similar results. For visualization, the reconstructed bead models were converted to electron density maps using real space convolution with a Gaussian kernel with the program Situs[14]. A kernel width of 6 Å and voxel spacing of 2 Å were employed.

In Vitro **Motility, Landing and Continuous Movement Assays:** Assays were conducted as described in Rock *et al*.[15]. Briefly, motors were attached with monoclonal anti-GFP antibody (Chemicon MAB3580) to nitrocellulose coated cover slips in the flow cell at concentrations ranging from ~10 pM to 1 nM. 0.1 μM TRITC phalloidin labeled actin was introduced in motility buffer consisting of 25 mM KCl, 25 mM imidazole pH 7.4, 4 mM $MgCl_2$, 1 mM EGTA, 10 mM DTT, 2 mM ATP, 4.5 μM calmodulin, an oxygen scavenging system of 10.8 μg ml^{-1} glucose oxidase, 1.8 μg ml^{-1} catalase, 0.4% (w/v) glucose, 1 mM trolox, and an ATP regeneration system of 1 mM phosphocreatine, 0.1 μg ml^{-1} phosphocreatine kinase. Movies were collect using a total internal reflection microscope[16] with 1 second frame rates and were scored for the number of filaments landing and moving more than 0.5 μm, the fraction of filaments running greater than their length, and the velocity with which filaments moved.

TIRF Motility Assays: Assays were conducted as described in Churchman *et al*.[16], with slight modifications. Briefly, biotin-BSA was placed onto the highly refracting coverslips made of NLAF21 (VA Optical Labs, San Anselmo, CA) in the flow cell, followed by a 1 mg ml^{-1} BSA wash, 0.5 mg ml^{-1} streptavidin, another BSA wash, 0.1 μM Alexa 633 phalloidin (Molecular Probes) labeled actin with ~1 in every 25 actin monomers biotin labeled at Cys374. Motors were labeled at a 1:1 ratio with anti-GFP antibody conjugated with multiple Cy3 fluorophores to enhance signal and introduced to flow cells in the motility buffer described above with the ATP concentration lowered to 80 μM. Movies were collected on the microscope described in Churchman *et al*.[16]. Movies were analyzed in imageJ (NIH, MD) by drawing a path along the actin filament and using the kymograph plugin to produce a plot of motor movement.

Optical Trap Assays: Assays were conducted as described in Rice *et al*.[17] and Altman *et al*.[18] with a few exceptions, notably that trapping was done without feedback resulting in non-constant loads on the motor. This was done because not all constructs assayed were processive and it was desirable to assay all motors under the same conditions. Briefly, motors were attached with monoclonal anti-GFP antibody (Chemicon MAB3580) to nitrocellulose coated cover slips studded with glass 1.5 μm platform beads in the flow cell at ~1 pM concentrations. 0.1 μM TRITC phalloidin labeled actin with all actin monomers biotin labeled at Cys374 was introduced in motility buffer consisting of 25 mM KCl, 25 mM imidazole pH 7.4, 4 mM $MgCl_2$, 1 mM EGTA, 10 mM DTT, 2 mM ATP, 4.5 μM calmodulin, 10 mM phalloidin, an oxygen scavenging system of 10.8 μg ml^{-1} glucose oxidase, 1.8 μg ml^{-1} catalase, 0.4% (w/v) glucose, 1% (v/v) β-mercaptoethanol, and an ATP regeneration system of 1 mM phosphocreatine, 0.1 μg ml^{-1} phosphocreatine kinase and 0.002% (v/v) of 1 μm neutravidin coated polystyrene trapping beads. Actin dumbbells were formed between two trapping beads and pulled taught. The dumbbell was placed over a platform and data collected if less than 1 in 10

platforms interacted with the actin. Positional data was collected at 10 kHz and trap stiffness ranged from 0.006–0.012 pN nm^{-1}. Binding events were determined by eye using a drop in the positional variance of the beads and the bead to bead correlation and transitions between processive steps were also scored by eye.

Supplementary References

1. Kikuno, R. et al. HUGE: a database for human KIAA proteins, a 2004 update integrating HUGEppi and ROUGE. *Nucleic Acids Res* **32**, D502-4 (2004).
2. De La Cruz, E.M., Ostap, E.M. & Sweeney, H.L. Kinetic mechanism and regulation of myosin VI. *J Biol Chem* **276**, 32373-81 (2001).
3. Xiong, A.S. et al. PCR-based accurate synthesis of long DNA sequences. *Nat Protoc* **1**, 791-7 (2006).
4. Chen, Y.H., Yang, J.T. & Chau, K.H. Determination of the helix and beta form of proteins in aqueous solution by circular dichroism. *Biochemistry* **13**, 3350-9 (1974).
5. Lipfert, J., Millett, I.S., Seifert, S. & Doniach, S. A Sample Holder for Small-Angle X-ray Scattering Static and Flow Cell Measurements. *Rev Sci Inst* **77**(2006).
6. Beno, M.A.a.J., G. and Engbretson, M. and Knapp, G. S. and Kurtz, C. and Zabransky, B. and Linton, J. and Seifert, S. and Wiley, C. and Montano, P. A. Basic Energy Sciences Synchrotron Radiation Center Undulator Sector at the Advanced Photon Source. *Nucl. Instr. & Meth. Phys. Res. A* **467-468**(2001).
7. Seifert, S., Winans, R.E., Tiede, D.M. & Thiyagarajan, P. Design and performance of a ASAXS instrument at the Advanced Photon Source. *Journal of Applied Crystallography* **33**, 782-784 (2000).
8. Guinier, A. La diffraction des rayons X aux tres petits angles: Application`a l'etude de phenomenes ultramicroscopiques. *Ann. Phys. (Paris)* **12**, 161-237 (1939).
9. Svergun, D. Determination of the regularization parameter in indirect-transform methods using perceptual criteria. *Journal of Applied Crystallography* **25**, 495-503 (1992).
10. Svergun, D.I. Restoring low resolution structure of biological macromolecules from solution scattering using simulated annealing. *Biophys J* **76**, 2879-86 (1999).
11. Svergun, D.I., Petoukhov, M.V. & Koch, M.H. Determination of domain structure of proteins from X-ray solution scattering. *Biophys J* **80**, 2946-53 (2001).
12. Kozin, M.B. & Svergun, D.I. Automated matching of high- and low-resolution structural models. *Journal of Applied Crystallography* **34**, 33-41 (2001).
13. Volkov, V.V. & Svergun, D.I. Uniqueness of ab initio shape determination in small-angle scattering. *Journal of Applied Crystallography* **36**, 860-864 (2003).
14. Wriggers, W. & Chacon, P. Using Situs for the registration of protein structures with low-resolution bead models from X-ray solution scattering. *Journal of Applied Crystallography* **34**, 773-776 (2001).
15. Rock, R.S., Rief, M., Mehta, A.D. & Spudich, J.A. In vitro assays of processive myosin motors. *Methods* **22**, 373-81 (2000).
16. Churchman, L.S., Okten, Z., Rock, R.S., Dawson, J.F. & Spudich, J.A. Single molecule high-resolution colocalization of Cy3 and Cy5 attached to macromolecules measures intramolecular distances through time. *Proc Natl Acad Sci U S A* **102**, 1419-23 (2005).

17. Rice, S.E., Purcell, T.J. & Spudich, J.A. Building and using optical traps to study properties of molecular motors. *Methods Enzymol* **361**, 112-33 (2003).
18. Altman, D., Sweeney, H.L. & Spudich, J.A. The mechanism of myosin VI translocation and its load-induced anchoring. *Cell* **116**, 737-49 (2004).